Novel kinematic model of articulated arm coordinate measuring machine with angular position measurement errors of rotary axes

S. Ibaraki (2)*, R. Saito

Graduate School of Advanced Science and Engineering, Hiroshima University, Kagamiyama 1-4-1, Higashi-Hiroshima 739-8527, Japan

Keywords:
Robot, Coordinate measuring machine (CMM)
Accuracy

A B S T R A C T

The measurement accuracy of an articulated arm coordinate measuring machine (AACMM) is determined by its kinematic model to estimate the end effector position from angular positions of rotary axes. In conventional studies, the Denavit–Hartenberg (DH) model, containing position and orientation errors of the rotary axis average lines as error sources, has been widely employed. This study first proposes a novel kinematic model including angular position measurement errors of rotary axes. To identify the proposed model, a new Single Point Articulation Test (SPAT) setup is presented with the R-Test to measure the stylus sphere's three-dimensional displacement. The prediction accuracy of the proposed model is experimentally evaluated.

1. Introduction

A conventional coordinate measuring machine (CMM) is typically in a room under strict thermal control, which continuously consumes significant amount of energy. For some metrological applications in manufacturing, "in-line" measurement, performed in or near manufacturing sites, can be an energy- and cost-effective alternative [1]. An articulated arm CMM (AACMM) is a CMM with a six- or seven-axis articulated arm structure (see Fig. 1). Each rotary axis is not motor-driven but a passive joint, whose angular position is measured by a rotary encoder. A human operator manually touches its end effector, typically a stylus sphere, to the target surface. Then, from the angular positions of rotary axes, the three-dimensional (3D) position of the end effector is estimated. This is the measuring principle of an AACMM. Compared to conventional CMMs of orthogonal linear axes, its portability is a strong advantage. Compared to its footprint, the measurable volume is much larger than conventional CMMs.

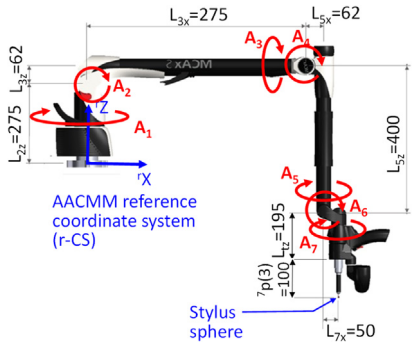

Fig. 1. Configuration of the seven-axis AACMM (Nikon MCAx20).

The measurement accuracy of AACMMs is often significantly worse than that of conventional CMMs of similar size [2]. A major uncertainty contributor is an error in the forward kinematic model, which is needed to calculate the end effector position from rotary axis angular positions. Numerous researchers have studied model-based compensation. Dupuis et al. [3] used the single point articulation test (SPAT) performed at conical sockets on a length gauge placed at various locations over the workspace. Rim et al. [4] used a plate of chamfered hole seats and the ball bar. Zhao et al. [5] used a 3D artefact. All of these works employed these tests to identify the Denavit-Hartenberg (DH) model. The DH model [6] is primitive but the most popular robot kinematics model. It contains position and orientation errors of the rotary axis average lines as error sources [7]. The *axis average line* represents the mean position and orientation of the axis of rotation [8].

For motorized six-axis serial manipulators, as reviewed in [9], numerous conventional studies are also based on the DH model, but some latest studies [10] presented the inclusion of *error motions* [8], which represent the variation in the position and orientation of the axis of rotation from its mean value. The inclusion of the joint or link stiffness can be seen as one of such extensions [11]. Similarly, for AACMMs, the modelling of the gravity-induced elastic deformation has been presented [12,13].

The measurement error of rotary axis angular position is typically caused by the graduation error of a rotary encoder scale. It varies with the angular position, and thus cannot be represented as the DH errors. The first original contribution of this paper is on the extension of the DH model to the angular position measurement error of rotary axes. For motorized serial manipulators, the angular positioning deviation of rotary axes is typically caused by the gear transmission error, and the author's group has proposed the model containing it. It has been first applied to a planar robot arm (angular positioning deviation can be identified by using a tracking interferometer [14] or a laser interferometer [15]) and then to a six-axis robot [16] (with axis-to-axis cross talk in [17]). This work can be seen as its extension to AACMMs.

* Corresponding author.
E-mail address: ibaraki@hiroshima-u.ac.jp (S. Ibaraki).

The major difference from motorized manipulators is in the measurement scheme. For a motorized manipulator, the end effector position was measured by using a tracking interferometer in [14,16,17]. Compared to the required accuracy for an AACMM, its measurement uncertainty may not be sufficiently small. This paper presents a scheme to identify the angular position measurement error of rotary axes based on a set of the SPATs, described in ISO 10360−12 [18]. In the conventional SPAT, due to finite stiffness of the spherical seat constraining the stylus sphere position, and since an AACMM is fully operated by a human, it is difficult to ensure that the stylus sphere displacement is constrained sufficiently small. This paper presents a nest of three displacement sensors (R-Test) to measure the stylus sphere's 3D displacement during the SPAT. The proposal of this modified SPAT procedure is the second original contribution of this paper.

2. Proposed AACMM kinematic model

2.1. Conventional kinematic model

This study considers a seven-axis AACMM configuration shown in Fig. 1. The kinematic model formulates the end effector position in the reference coordinate system (r-CS), denoted by ${}^r\hat{p}\in\Re^3$ (the left-hand side superscript represents the CS), when the angular position of the A_n-axis (n = 1, .., 7) is given by $\theta_n{}^*\in\Re$:

$$\begin{bmatrix} {}^r p \\ 1 \end{bmatrix} = {}^rT_7 \cdot \begin{bmatrix} {}^7 p \\ 1 \end{bmatrix} \tag{1}$$

$${}^rT_7 = {}^rT_1 \cdot {}^1T_2 \cdot {}^2T_3 \cdot {}^3T_4 \cdot {}^4T_5 \cdot {}^5T_6 \cdot {}^6T_7 \tag{2}$$

$${}^rT_1 = D_c(\theta_1)$$

$${}^1T_2 = D_x(\delta x_{21})D_z(L_{2z})D_a(\alpha_{21})D_b(\theta_2)$$

$${}^2T_3 = D_x(L_{3x})D_y(\delta y_{32})D_Z(L_{3z}+\delta z_{32})D_b(\beta_{32})D_c(\gamma_{32})D_a(\theta_3+\Delta\theta_{30})$$

$${}^3T_4 = D_x(\delta x_{43})D_z(\delta z_{43})D_c(\gamma_{43})D_b(\theta_4+\Delta\theta_{40})$$

$${}^4T_5 = D_x(L_{5x}+\delta x_{54})D_y(\delta y_{54})D_z(-L_{5z})D_a(\alpha_{54})D_c(\theta_5+\Delta\theta_{50})$$

$${}^5T_6 = D_x(\delta x_{65})D_z(\delta z_{65})D_a(\alpha_{65})D_b(\theta_6+\Delta\theta_{60})$$

$${}^6T_7 = D_x(L_{7x}+\delta x_{76})D_y(\delta y_{76})D_a(\alpha_{76})D_c(\theta_7)$$

where $D_*(\dagger)\in\Re^{4\times4}$ denotes the homogeneous transformation matrix (HTM) representing the linear translation to the X-, Y-, and Z-directions (for *: x, y, z) by the distance $\dagger\in\Re$, or the rotation around the X-, Y-, and Z-axes (for *: a, b, c) by the angle †. Their formulation is given in [7] and is omitted in this paper. $L_*\in\Re$ represents the nominal link length shown in Fig. 1. The other 22 parameters, for example, δx_{21}, α_{21}, $\Delta\theta_{30}$, …, are the DH parameters. Their definition is similar as those in the six-axis robot in [16] and is omitted in this paper. ${}^7p\in\Re^3$ is the tool vector given in the A_7-axis CS. The proposed algorithm also identifies it.

The kinematic model (1) can be derived based on the well-established HTM-based CS transformation theory [7] and is not a part of this study's new contributions.

2.2. Proposed model with angular position measurement errors

This study's first original contribution is in the inclusion of the angular position measurement errors of rotary axes in the kinematic model (1). The measurement error of a rotary encoder varies with the angular position. For the prescribed set of A_n-axis angular positions, $\theta_{n,map}{}^*(i_n)\in\Re$, where $i_n\in\Re$ is the index number (i_n=1, …, N_n), the angular position measurement error is denoted by $\Delta\theta_{n,map}(i_n)$. It is represented in a look-up table format with i_n as the input. When the A_n-axis rotary encoder readout is arbitrarily given by $\theta_n{}^*$, the angular position measurement error, $\Delta\theta_n$, is calculated by linearly interpolating $\Delta\theta_{n,map}(i_n)$. Then, $\theta_n{}^*+\Delta\theta_n$ is substituted to the model (2).

The step size of the nominal angular positions, $\theta_{n,map}{}^*(i_n)$, should be determined based on prior knowledge on possible error sources. The concentricity error of the scale to the axis rotation results in a sinusoidal measurement error of the period 2π. The scale distortion and radial/tilt error motions can give higher order harmonics. Ref. [19] reports that seven points per cycle will remove approximately 90% of the measurement error. In the experiment in Section 4, the step size of $\theta_{n,map}{}^*(i_n)$ is 5° for all the axes.

3. Identification of angular position measurement errors

3.1. Proposed test procedure

For any given stylus sphere position, there are countless possible postures that an AACMM can take. As the stylus sphere is constrained at a single point, a human operator changes the AACMM poses, with the A_1- to A_7-axis angular positions continuously logged. Such a test is called the SPAT in ISO 10,360−12 [18]. This paper adopts this test.

Due to finite stiffness of a spherical seat to constrain the stylus sphere, and since an AACMM is fully operated by a human operator, it is often difficult to ensure that the stylus sphere's displacement is sufficiently small during the SPAT. Indeed, in the experiment in Section 4, Fig. 5 shows that the stylus sphere was displaced by 15 μm at maximum during the SPAT, which may not be acceptable compared to the required accuracy for AACMMs.

To address this issue, we propose the application of the R-Test, shown in Fig. 2, to the SPAT. The R-test was first proposed by Weikert [20] and its application to error source identification for five-axis

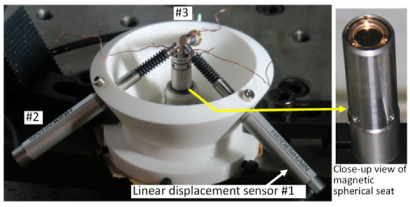

Fig. 2. R-Test sensors nest for the SPAT. The magnetic spherical seat for the telescoping ball bar, Renishaw QC-20 W, is used.

machine tools has been well established [21]. The AACMM stylus sphere is constrained in a magnetic spherical seat. Three tactile linear displacement sensors measure its 3D displacement during the SPAT. Fig. 3 shows the proposed SPAT setup.

Fig. 3. Proposed SPAT setup. As end effector orientation is changed, stylus sphere displacement is continuously measured by the R-Test.

To cover larger angular range of rotary axes, we propose performing the proposed SPAT at multiple locations. Furthermore, to measure not only the sphere's relative displacement at each R-Test location, but also its "absolute" position in a single CS, the R-Test sensors nest is fixed on a machine tool worktable, and its location is measured by using the machine tool. A precision sphere is attached to the machine spindle, and its position in the machine CS is searched, where the three linear displacement sensors are zeroed (see Fig. 4a). The positioning error of the machine tool is assumed sufficiently small

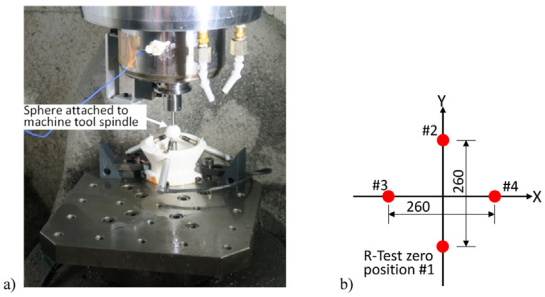

Fig. 4. a) Setup to measure the position of the R-Test sensors nest by using machine tool. b) R-Test locations in the experiment in Section 4.

compared to the accuracy required for the AACMM. In the experiment in Section 4, the machine tool's 2D positioning error was measured by using a 2D digital scale and it was smaller than 3 μm over the range X260 × Y260 mm (see Fig. 4b).

Suppose that the zero position of the R-Test at the m-th location is measured as ${}^{\mathrm{mt}}p_0(m) \in \Re^3$ in the machine tool CS (MT-CS). When the i_{m}-th sphere displacement, ${}^{\mathrm{mt}}\sim p(m, i_m)$ (i_{m}=1, …, $N(m)$), is measured by the R-Test, relative to its zero position,

$$ {}^{\mathrm{mt}}p(m, i_m) = {}^{\mathrm{mt}}p_0(m) + {}^{\mathrm{mt}}\sim p(m, i_m) \tag{3} $$

represents the measured stylus sphere position in the MT-CS.

3.2. Identification of DH parameters and rotary axis angular position measurement errors

The orientation of the AACMM r-CS, shown in Fig. 1, in the MT-CS, is unknown. The proposed algorithm identifies it. Suppose that the r-CS can be transformed to the MT-CS by rotating α_0, β_0, γ_0 around X, Y and Z-axes. Define X_0=[α_0, β_0, γ_0].

Convert the predicted stylus sphere position, ${}^{r}\hat{p}(m, i_m)$, given in the r-CS by Eq. (1), to the MT-CS by:

$$ {}^{\mathrm{mt}}\hat{p}(m, i_m) = D_b(\beta_0)D_a(\alpha_0)D_c(\gamma_0)[{}^{r}\hat{p}\,(m, i_m) - {}^{r}\hat{p}(m_0, i_{m0})1] \tag{4} $$

where m_0 and i_{m0} represent the initial position, e.g. m_0 = i_{m0} = 1. The objective of the present algorithm is to identify 1) X_0, 2) $X_{\mathrm{dh}} \in \Re^{25}$, containing 25 D-H parameters in Eq. (2) (including ${}^{7}p$), and 3) the angular position measurement error of A_n-axis, X_n, defined by:

$$ X_n = \begin{bmatrix} \Delta\theta_{n,\mathrm{map}}(i_1) \\ \vdots \\ \Delta\theta_{n,\mathrm{map}}(i_{N_n}) \end{bmatrix} \in \mathbb{R}^{N_n \times 1} \tag{5} $$

for all the rotary axes, n = 1, …, 7. They can be identified by solving the following problem:

$$ \min_{X_0, X_{\mathrm{dh}}, X_1, \ldots, X_7} \sum_{m=1}^{N_m} \sum_{i_m=1}^{N(m)} \| {}^{\mathrm{mt}}\hat{p}(m, i_m) - \left({}^{\mathrm{mt}}p(m, i_m) - {}^{\mathrm{mt}}p(m_0, i_{m0}) \right) \|_2^2 \tag{6} $$

Eq. (6) can be locally solved by the Newton method.

4. Experiment

4.1. Experimental setup

The seven-axis AACMM, Nikon MCAx20 (Fig. 1), was tested. For the R-Test, the linear displacement sensors, ST1288 by Heidenhain (system accuracy: ±1μm), were used. The SPAT was performed at four locations shown in Fig. 4b on the machining centre worktable.

4.2. Identification of angular position measurement errors

First, Fig. 5 shows the stylus sphere displacement profile in the XY plane measured during the SPAT at the R-Test location #3 (see Fig. 4b). Although the sphere was constrained by the magnetic spherical seat, it was displaced by 15 μm in the XY plane at maximum. Compared to the target measurement accuracy of the AACMM, this is

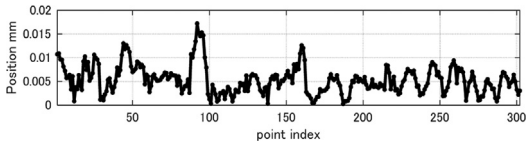

Fig. 5. Stylus sphere displacement profiles in the XY plane measured by the R-Test during the SPAT at location #3.

not negligibly small. Fig. 5 clarifies the necessity of the R-Test to improve the accuracy of the SPAT.

By applying the proposed algorithm in Section 3.2, the angular position measurement error profiles of A_n-axes, $\Delta\theta_{n,\mathrm{map}}(i_n)$ (n = 1 to 6), were identified. Fig. 6 shows A_1- to A_3-axis profiles only.

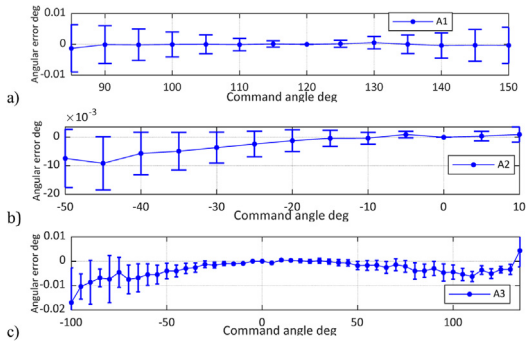

Fig. 6. Angular position measurement error profiles (blue dots) of a) A1-axis, b) A2-axis, and c) A3-axis, identified by the proposed scheme. Vertical error bars represent the uncertainty (k = 1) assessed in Section 5.

4.3. Estimation accuracy evaluation by length measurements

The position estimation accuracy by the proposed model was investigated by length measurement tests. An artefact steel bar with three conical sockets (A, B and C), between which the distance is pre-calibrated, was used. Fig. 7 shows the experimental setup. The bar was placed in total seven locations shown in Fig. 8. The AACMM stylus sphere was put into the sockets, and similarly as the SPAT, the end effector orientation was varied at each socket.

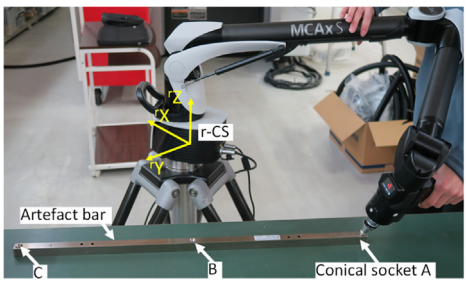

Fig. 7. Artefact bar with conical sockets at location 1 in Fig. 8.

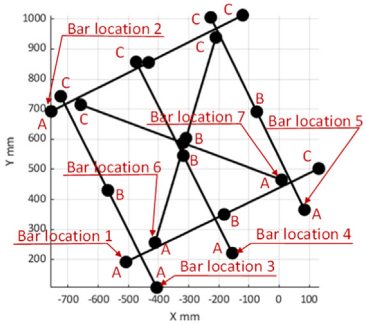

Fig. 8. Bar locations in the r-CS. A, B and C represents the conical sockets. (X, Y)=(0, 0) represents the origin of the r- CS (see Fig. 1).

Fig. 9 compares the estimation error of the mean distances between a) A and B, and b) A and C, in reference to their pre-calibrated distances (A-B: 361.775 mm, A-C: 711.211 mm). To estimate the stylus sphere

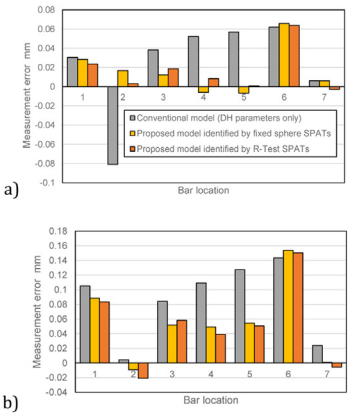

Fig. 9. Measurement errors of the distances between the conical sockets a) A and B and b) A and C at bar locations 1 to 7 in Fig. 8.

position by Eq. (1), the three models are compared: 1) (grey) the conventional DH model, containing 25 DH parameters only. The DH parameters were identified based on the proposed SPATs with the R-Test. 2) (yellow) The proposed model with the DH parameters and A1-A7 axis angular position measurement errors, identified by the conventional fixed-sphere SPATs. The mean value of the sphere displacement profile measured by the R-Test was taken at each SPAT. 3) (red) The proposed model identified by the SPATs with the R-Test.

Compared to the conventional DH model (grey), the proposed model (orange) shows a significantly smaller measurement error at 9 tests out of 14 (Locations 2, 3, 4, 5, 7 for A-B, and 2, 4, 5, 7 for A-C). The difference is minor in other five tests. Comparing yellow and orange bars, the contribution of the R-Test on the identification of angular position measurement errors is minor, but a slight improvement can be observed in eight tests (Locations 1, 2, 5, 6, 7 for A-B, and 1, 4, 5, 6 for A-C). It is interesting to observe that the models did not significantly influence at Locations 1 and 6. This is probably due to error sources that are not considered in this paper, such as the elastic deformation of AACMM structural parts.

5. Uncertainty analysis

In the SPAT, all the error sources influence the stylus sphere position. Depending on test conditions, the uncertainty in the estimation of some error sources can be higher. Thus, the uncertainty analysis is essential.

The following uncertainty contributors are considered: the measurement uncertainty (k = 1) of the sphere's displacement by the R-Test is assessed as σ_{RTest}=2 μm, and the uncertainty (k = 1) in the R-Test locations is assessed as $\sigma_{\mathrm{location}}$=3 μm, which can be caused by the machine tool's positioning error. Their propagation to the uncertainty in the estimated DH parameters and angular position measurement errors in each axis was assessed by the Monte Carlo simulation, as is well established in indirect error identification schemes for machine tools [22].

In Fig. 6, vertical error bars represent the uncertainty (k = 1) in the estimated angular position measurement error. The uncertainty is significantly larger in some angular ranges, likely due to insufficient number of data with these poses involved in the SPATs. By optimizing the test conditions, e.g. the R-Test locations and the poses in the SPATs, the uncertainty may be reduced. This is left for our future research.

6. Conclusion

Contributions of this paper can be summarized as follows:

- New SPAT procedure was proposed. Due to finite stiffness of the spherical seat, the stylus sphere may not be completely constrained in the conventional SPAT setup. The R-Test was applied to measure the stylus sphere's 3D displacement.
- The new kinematic model, containing the angular position measurement error of rotary axes as error sources, was proposed. The experiment showed that the measurement error of the AACMM was significantly reduced from the conventional DH model.
- The contribution of the R-Test on the identification of rotary axis angular position measurement errors was minor. In the present experiment, the sphere displacement in the SPATs, measured by the R-Test, was at maximum 15 μm. Although it may not be significantly large compared to the AACMM's measurement error, it is important to actually measure the sphere displacement and explicitly consider it in the model identification.

Declaration of Competing Interest

The authors declare that they have no known competing financial interests or personal relationships that could have appeared to influence the work reported in this paper.

Acknowledgement

This work was supported in part by JSPS KAKENHI (JP 21H01228).

References

[1] Mutilba U, Gomez-Acedo E, Kortaberria G, Olarra A, Yagüe-Fabra JA (2017) Traceability of On-Machine Tool Measurement: a Review. *Sensors* 17:1605–1642.
[2] Mutilba U, Kortaberria G, Olarra A, Gutiérrez A, Gomez-Acedo E, Zubieta M (2013) Performance Calibration of Articulated Arm Coordinate Measuring machine. *Procedia Engineering* 63:720–727.
[3] Dupuis J, Holst C, Kuhlmann H (2017) Improving the kinematic calibration of a coordinate measuring arm using configuration analysis. *Precision Engineering* 50:171–182.
[4] Rim CH, Rim CM, Kim JG, Chen G, Pak JS (2019) A calibration method of portable coordinate measuring arms by using artifacts. *MAPAN-Journal of Metrology Society of India* 34:1–11.
[5] Zhao HN, Yu LD, Xia HJ, Li WS (2018) 3D artifact for calibrating kinematic parameters of articulated arm coordinate measuring machines. *Measurement Science and Technology* 29(6):065009.
[6] Denavit J, Hartenberg RS (1955) A kinematic notation for lower-pair mechanisms based on matrices. *ASME J. Appl. Mech.* : 215–221.
[7] Alam MM, Ibaraki S, Fukuda K (2021) Kinematic Modeling of Six-Axis Industrial Robot and its Parameter Identification: a Tutorial. *International Journal of Automation Technology* 15(5):599–610.
[8] ISO 230-1:2012, Test code for machine tools – Part 1: geometric accuracy of machines operating under no-load or quasi-static conditions.
[9] Ibaraki S, Theissen NA, Archenti A, Alam MM (2021) Evaluation of Kinematic and Compliance Calibration of Serial Articulated Industrial Manipulators. *International Journal of Automation Technology* 15(5):567–580.
[10] Ma L, Bazzoli P, Sammons PM, Landers RG, Bristow DA (2018) Modeling and calibration of high-order joint-dependent kinematic errors for industrial robots. *Robotics and Computer-Integrated Manufacturing* 50:153–167.
[11] Kamali K, Bonev IA (2019) Optimal Experiment Design for Elasto-Geometrical Calibration of Industrial Robots. *IEEE/ASME Transactions on Mechatronics* 24(6):2733–2744.
[12] Hu Y, Huang W, Hu PH, Liu WW, Ye B (2019) Design and Validation of a Self-Driven Joint Model for Articulated Arm Coordinate Measuring Machines. *Applied Science* 9:3151–3162.
[13] El Asmai S, Hennebelle F, Coorevits T, Vincent R, Fontaine JF (2020) Proposition of a periodic verification test for Articulated Arm Coordinate Measuring Machines using a small 3D artefact. *Measurement* 154:107472.
[14] Zhao N, Ibaraki S (2022) Novel kinematic model of a SCARA-type robot with bi-directional angular positioning deviation of rotary axes. *The International Journal of Advanced Manufacturing Technology* 120:4901–4915.
[15] Ibaraki S, Usui R (2022) A novel error mapping of bi-directional angular positioning deviation of rotary axes in a SCARA-type robot by "open-loop" tracking interferometer measurement. *Precision Engineering* 74:60–68.
[16] Alam MM, Ibaraki A, Fukuda K, Morita S, Usuki H, Otsuki N, Yoshioka H (2022) Inclusion of Bidirectional Angular Positioning Deviations in the Kinematic Model of a Six-DOF Articulated Robot for Static Volumetric Error Compensation. *IEEE/ASME Transactions on Mechatronics* 27(6):4339–4349.
[17] Ibaraki S, Fukuda K, Alam MM, Morita S, Usuki H, Otsuki N, Yoshioka H (2021) Novel six-axis robot kinematic model with axis-to-axis crosstalk. *CIRP Annals* 70(1):411–414.
[18] ISO 10360-12:2016, Geometrical product specifications (GPS) — Acceptance and reverification tests for coordinate measuring systems (CMS) — Part 12: Articulated arm coordinate measurement machines (CMM)
[19] Renishaw white paper: The accuracy of rotary encoders, https://www.renishaw.com/en/the-accuracy-of-rotary-encoders–47130 (accessed on Jan. 2023)
[20] Weikert S (2004) R-Test, a New Device for Accuracy Measurements on Five Axis Machine Tools. *Annals of the CIRP* 53(1):429–432.
[21] Hong C, Ibaraki S (2012) Graphical presentation of error motions of rotary axes on a five-axis machine tool by static R-test with separating the influence of squareness errors of linear axes. *International Journal of Machine Tools and Manufacture* 59:24–33.
[22] Ibaraki S, Okumura R (2021) A machining test to evaluate thermal influence on the kinematics of a five-axis machine tool. *International Journal of Machine Tools and Manufacture* 163:103702.